# Supporting Information

## Ultra-flexible and Waterproof Perovskite Photovoltaics for Washable Power Source Applications

*Zengqi Huang[a], Juan Long[b], Runying Dai[a], Xiaotian Hu[b], Liyun Le[c], Xiangchuan Meng[b], Licheng Tan*[b], Yiwang Chen*[a,b]*

[a]Institute of Advanced Scientific Research (iASR), Key Laboratory of Functional Organic Small Molecules for Ministry of Education, Jiangxi Normal University, 99 Ziyang Avenue, Nanchang 330022, China

[b]Institute of Polymers and Energy Chemistry (IPEC), Nanchang University, 999 Xuefu Avenue, Nanchang 330031, China

[c]State Key Laboratory of Nuclear Resources and Environment, East China University of Technology, 418 Guanglan Avenue, Nanchang 330013, China

Corresponding author. E-mail: ywchen@ncu.edu.cn (Y. C.); tanlicheng@ncu.edu.cn (L. T.).

**Experimental Section**

**Materials.** Lead (II) iodide ($PbI_2$, 99.999% purity) were purchased from Afar Aesar. Polyethyleneimine (PEI), poly(ethylene-*co*-vinyl acetate) (EVA, vinyl acetate 40 wt%), Nickel(II) nitrate hexahydrate ($Ni(NO_3)_2 \cdot 6H_2O$), anhydrous chlorobenzene (CBZ), anhydrous N,N-dimethylformamide (DMF) and anhydrous dimethyl sulfoxide (DMSO) were purchased from Sigma-Aldrich. Methylamine iodide (MAI) (>98% purity) and [6,6]-phenyl-$C_{61}$-butyric acid methyl ester ($PC_{61}BM$) were purchased from Xi'an p-OLED Corp. All the chemicals and materials were used as received without further purification.

**$NiO_x$ nanoparticles synthesis.** $NiO_x$ nanoparticles were synthesized using a previously reported procedure.[1-3] $Ni(NO_3)_2 \cdot 6H_2O$ was firstly dispersed in deionized water. Then, sodium hydroxide (NaOH) solution (10 mol/L) was dropwise adding into the solution in order to adjust pH to ~10. The obtained colloidal precipitation was centrifuged after stirring for 5 min, then the precipitation was cleaned with deionized water and dried at 80 °C for 6 h. Finally, the obtained colloidal precipitation was calcined at 270 °C for 2 h to obtain the $NiO_x$ powders.

**Device fabrication.** PET and PET-ITO (sheet resistance of 70 Ω $sq^{-1}$) were ultrasonically cleaned with abstergent aqueous solution, deionized water, acetone, and isopropyl alcohol for 20 min and then, dried with a nitrogen stream before next use. All the flexible substrates were cleaned with air plasma for 5 min. Thin films of polydimethylsiloxane (PDMS) was bonded to a glass substrate as a rigid support. All the flexible substrates were attached on the glass/PDMS during the whole fabrication process before self-encapsulation. For the ultra-flexible devices, a highly conductive PEDOT:PSS (Heraeus CLEVIOS™ PH1000) aqueous solution was spin-coated onto the PET substrates at 3000 rpm for 1 min, and subsequently annealed at 120 °C for 10 min. For the front stack, a ~20 nm $NiO_x$ film was prepared by spin coating at 2000 rpm for 30 s on the substrate, and then annealed at 120 °C for 20 min. The perovskite ($CH_3NH_3PbI_3$) precursor solution was prepared by mixing $PbI_2$ and $CH_3NH_3I$ with a

molar ration of 1:1 in DMF/DMSO (9:1, v/v) with stirring 2 h at 60 °C before used. The perovskite precursor solution was spin-coated at 4000 rpm for 25 s, following with a dropping of EVA solution (0-8 mg $mL^{-1}$ in chlorobenzene) after spin coating process for 10 s. Then, the perovskite precursor coated substrate was annealed on a hot plate at 80 °C for 1 min and 110 °C for 10 min. For the back stack, 50 μL of PEI solution (0.1 wt%) was spin-coated on the substrate at 3000 rpm for 30 s and followed by vacuum treatment. Then, 50 μL of PCBM solution (20 mg $mL^{-1}$) was spin-coated on the film at 1000 rpm for 30 s. The final devices were fabricated by laminating the front and back stacks. The active area, as defined by the overlap of ITO, is 0.19 $cm^2$. Aperture area of the mask used for selective illumination of the device, either during light-soaking or *J-V* measurement is 0.2 $cm^2$. For the conventional devices with Ag electrode, the $NiO_x$ film and perovskite film were sequentially deposited by the same method as above. Then, 20 mg $mL^{-1}$ PCBM was deposited via spin coating at 2000 rpm for 30s. Finally, the device was completed upon the evaporation of Ag contact electrodes (90 nm) at a vacuum level of $10^{-7}$ Torr through shadow masks. The active area of the conventional devices was fixed at 0.04 $cm^2$.

**Self-encapsulation process.** The flexible hot pressing lamination and self-encapsulation were accomplished by a temperature controllable laminator. It was consisted of an upper fixed crossbar and lower crossbar movable by a spindle drive. Both the front stack and back stack were placed on the top of each other in between the planar pates. Notably, the two separated-stacks were placed between two sheets of thin PET with or without EVA modified on each side. The optimum lamination temperature of 120 °C is carried out. And the flexible lamination of the perovskite solar cells was performed at a constant pressure. To explore the performance differences resulted from different pressure values, the statistical efficiencies of the devices with different pressure were shown below:

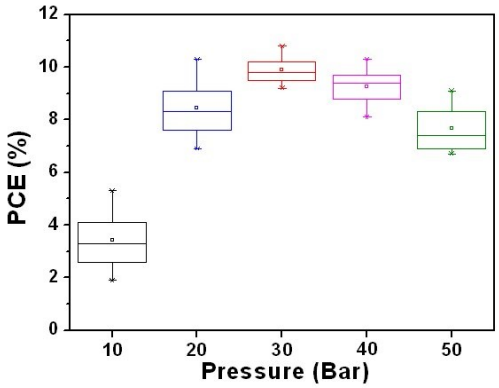


The measurement was carried out under AM 1.5G simulated solar light, 100 mW $cm^{-2}$. 10 devices were measured for statistical analysis in each case. The results demonstrate that the favourable value of the lamination pressure is 30 bar in our experiment.

**PDMS encapsulation process.** For this method, the flexible perovskite solar cells were fabricated in conventional structure with Ag electrode. PDMS and curing agent, trimethylsiloxyterminated poly(methylhydro-siloxane) polymers were purchased from Dow Corning™. The two components were mixed at a ratio of 10:1. The PDMS solution was continuously vacuumized in a vacuum drying oven to eliminate the bubbles. The PDMS was dropped on the top of the perovskite solar cells followed by covering a piece of PET, and baked at 80 °C till the entire solidification PDMS. The schematic illustration of the *f*-PSCs encapsulated by PDMS is shown below:

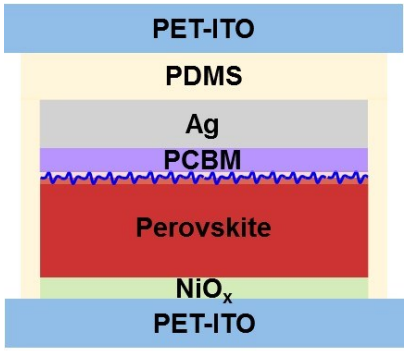


**EVA encapsulation process.** For this method, the flexible perovskite solar cells were fabricated in conventional structure with Ag electrode. EVA was dissolved in CBZ to form the glue solution by ultrasonic dispersion. The EVA was dropped on the top of

the perovskite solar cells followed by covering a piece of PET, and baked at 90 °C till the entire solidification EVA. The schematic illustration of the *f*-PSCs encapsulated by EVA is shown below:

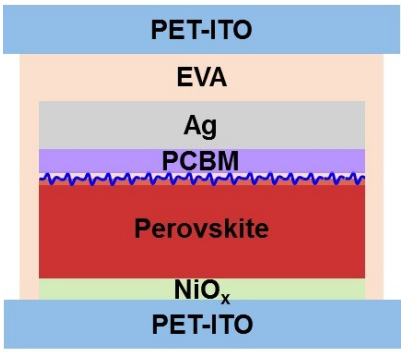


**Characterization.** Scanning electron microscopy (SEM) images were measured by JEOL (JSM-7500F, Japan) at an acceleration voltage of 5 kV. X-ray diffraction (XRD) measurements were recorded by using a D8-Discover 25 diffractometer (Bruker). The ultraviolet-visible (UV-Vis) spectra were recorded on a PerkinElmer Lambda 750 spectrophotometer. The steady-state photoluminescence (PL) measurements were carried out by a steady state and lifetime spectrometer (FLS920, Edinburgh Instruments Ltd.). The Young's Model studies were measured using the peak-force model of atomic force microscopy (AFM). The electrical impedance spectroscopy (EIS) was performed with Zahner electrochemical workstation. The illuminated current density-voltage (*J-V*) curves were characterized using Keithley 2400. The currents were measured under 100 mW $cm^{-2}$ simulated AM 1.5G irradiation (Abet Solar Simulator Sun 2000). All the measurements were performed under ambient atmosphere at room temperature. The forward scan range is from 0 V to 1.2 V and the reverse scan range is from 1.2 V to 0 V, with 8.0 mV for each step. The scan rate is 200 mV $s^{-1}$ and the delay time is 30 ms. The *J-V* curves are recorded first to verify the voltage at maximum power point (MPP). Then an external bias identical to the voltage at MPP in initial *J-V* curves is applied on the devices. By monitoring the current density under AM 1.5 G illumination, the stabilized power output is obtained through multiplying the current density by the applied bias. The repeated bending cycles were performed by a stretching machine (Beijing Zhongke J&M), which was

actuated by a stepper motor. The crumpling durability test was performed by randomly squeezing the device as shown in Supplementary Video. The external quantum efficiency (EQE) spectra were detected under monochromatic illumination (Oriel Cornerstone 260 1/4 m monochromator equipped with Oriel 70613NS QTH lamp), and the calibration of the incident light was performed with a monocrystalline silicon diode. The Pb concentration in the contaminated water were determined using an Agilent 7900 ICP-MS instrument.

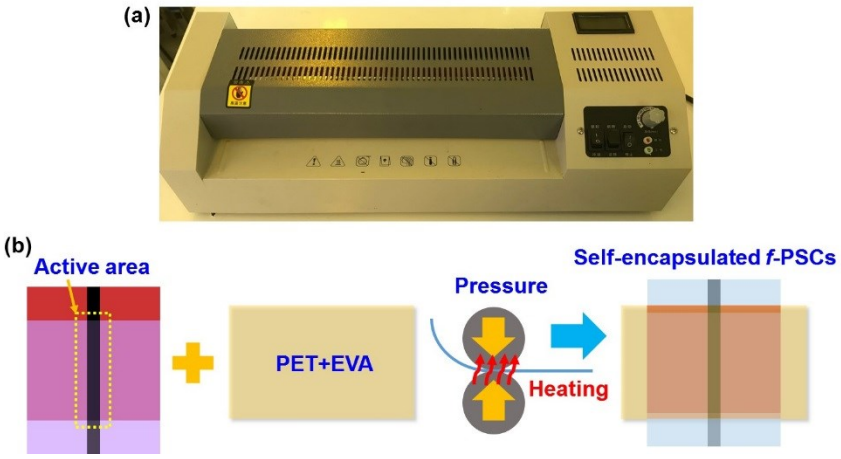


**Figure S1.** a) Photographic image of the temperature controllable laminator. b) Schematic illumination of the self-encapsulation process.

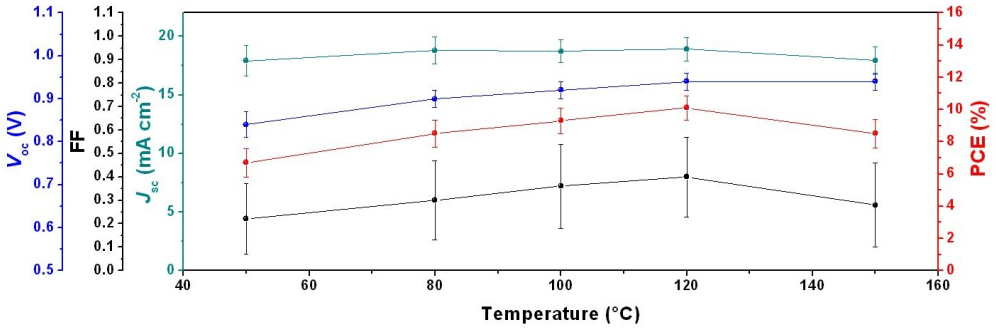


**Figure S2.** Photovoltaic parameters of the self-encapsulated flexible PSCs with the structure of PET/EVA/PET-ITO/$NiO_x$/Pervoskite/EVA/PCBM/PEI/PET-ITO/ PET/EVA upon different lamination temperatures.

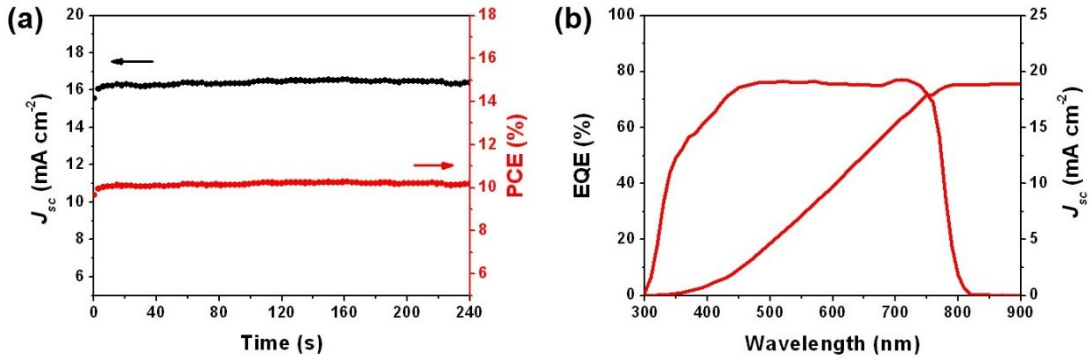


**Figure S3.** a) Stabilized output power and b) external quantum efficiency (EQE) spectrum of the champion self-encapsulated flexible PSC with the structure of PET/EVA/PET-ITO/$NiO_x$/Pervoskite/EVA/PCBM/PEI/PET-ITO/PET/EVA.

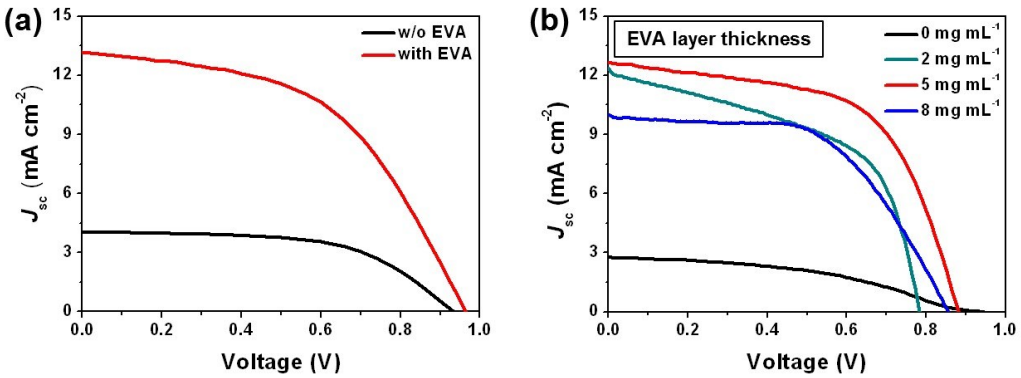


**Figure S4.** *J-V* curves of the self-encapsulated flexible PSCs (with the structure of PET/EVA/PET-ITO/$NiO_x$/Pervoskite/PCBM/PET-ITO/PET/EVA) fabricated with or without EVA bonding layer. b) *J-V* curves of the self-encapsulated devices fabricated with different thickness of EVA layer.

The f-PSC laminated with EVA bonding layer has a significant improvement in the photovoltaic performance (**Figure S4a**). **Figure S4b** shows the *J-V* curves of the laminated f-PSCs with EVA layers of different thickness which are adjusted by different concentration of EVA solution. The optimum devices are made by 5 mg mL$^{-1}$ EVA solution, and the EVA layer thickness is estimated to be ~2 nm. Further increasing the thickness of EVA layer will significantly reduce the device performance (especially the $J_{sc}$), owing to the reduced electron transport rate resulting from excessive EVA. These results demonstrate that the EVA bonding layer plays an important role in facilitating the interface contact between the front and back stacks.

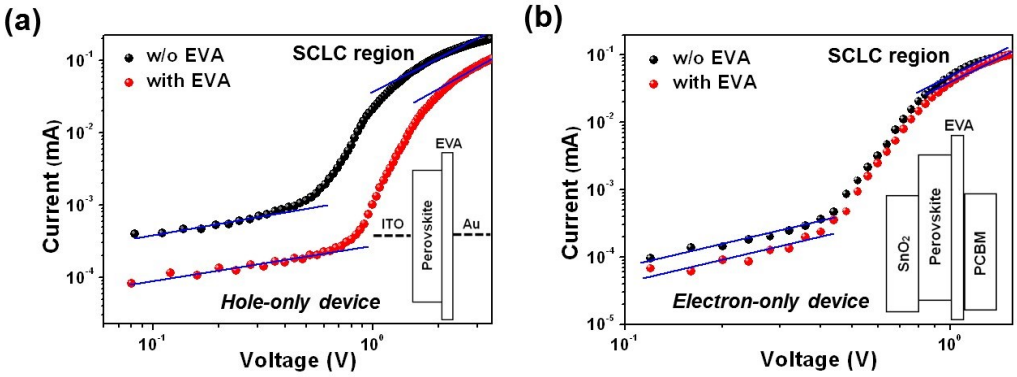


**Figure S5.** Dark current-voltage (*I-V*) characteristics of a) hole-only devices and b) electron-only devices. The insets show the structures of hole-only and electron-only devices, respectively.

The function of the EVA layer in carrier transfer is also confirmed by using the single-carrier devices with or without EVA layer. The structure of the hole only devices is ITO/perovskite/with or without EVA/Au, and the structure of the electron only devices is ITO/$SnO_2$/perovskite/with or without EVA/PCBM/Ag, which are shown in **Figure S5**. The EVA layer can spatially transport electrons and block holes, which balance the charge transfer in the cell.

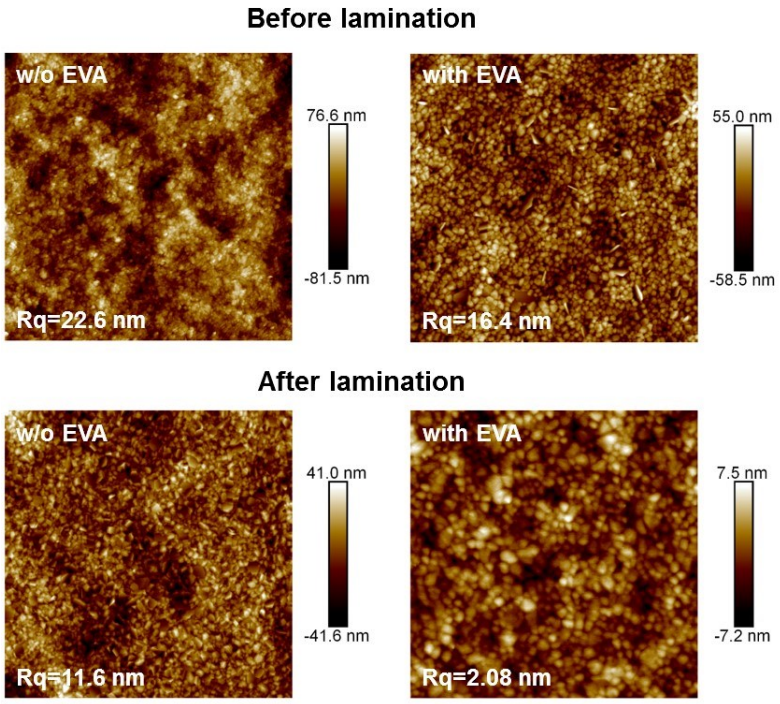


**Figure S6**. Atomic force microscope (AFM) images of perovskite films (w/o or with EVA layer) before and after flexible lamination.

We conduct atomic force microscope (AFM) to measure the surface roughness (as shown in **Figure S6**). The surface roughness of perovskite layer reduces from 22.6 nm to 16.4 nm by EVA treatment, and this surface roughness further reduces to 2.08 nm after flexible lamination. The lower surface roughness and unclear morphology of perovskite layer indicates that a thin EVA layer is formed upon the perovskite layer, thus resulting in a smoother surface morphology.

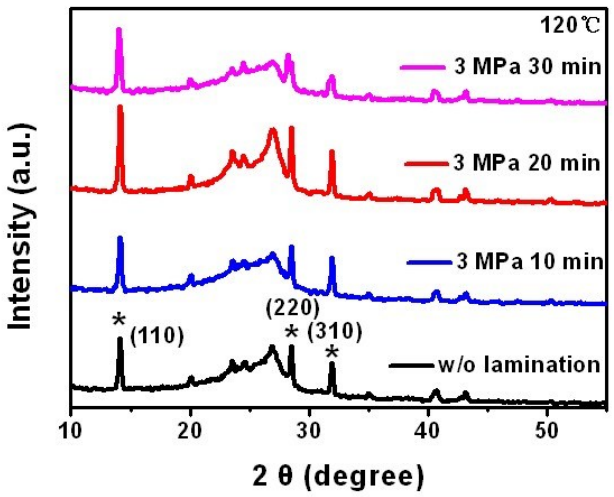


**Figure S7.** X-ray diffraction (XRD) patterns of perovskite films fabricated on PET-ITO after lamination at 120 °C with different time.

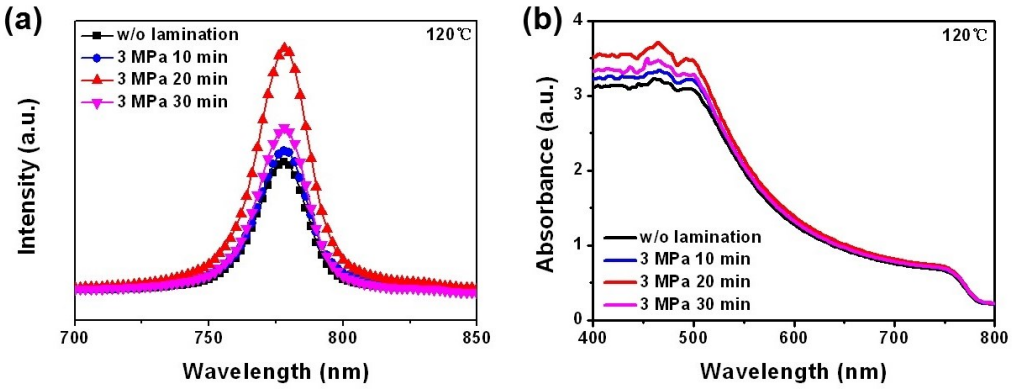


**Figure S8.** a) Steady-state PL and UV-Vis absorption spectra of perovskite films fabricated on PET-ITO after lamination at 120 °C with different time.

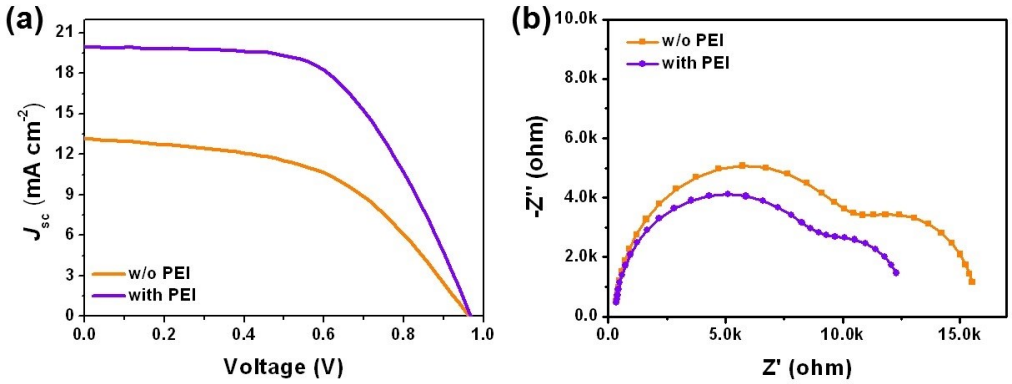


**Figure S9.** a) *J-V* curves and b) Nyquist plots of the self-encapsulated flexible PSCs (with the structure of PET/EVA/PET-ITO/$NiO_x$/Pervoskite/EVA/PCBM /PET-ITO/PET/EVA) fabricated with or without using PEI buffer layer between PCBM and PET-ITO.

The Nyquist plots (**Fig. S9b**) of f-PSCs with or without PEI both consist of two frequency regions. The low frequency element reflects the device resistance ($R_s$), and the high frequency element reflects the charge transfer resistance ($R_c$), respectively. Compared to the reference device, the decreased $R_c$ in PEI based device means that PEI buffer layer can facilitate the interfacial charge carrier transport between PCBM and the transparent electrode, and leads to the reduction of $R_s$.

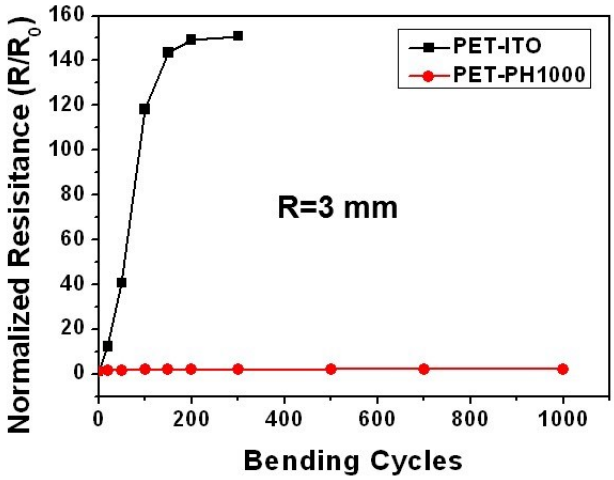


**Figure S10.** Normalized resistance of flexible electrodes as a function of bending cycles with a radius of 3 mm.

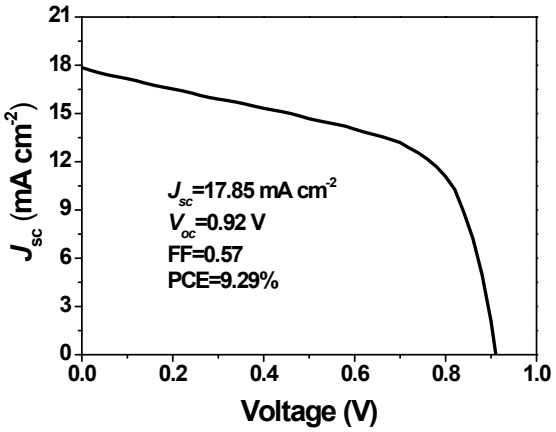


**Figure S11.** *J-V* curve of the ultra-flexible and self-encapsulateddevice with the structure of PET/EVA/PET-PH1000/$NiO_x$/Pervoskite/EVA/PCBM/PEI/PET-PH1000/ PET/EVA.

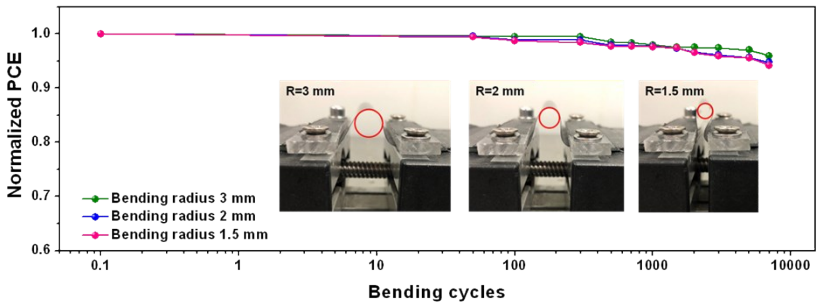


**Figure S12.** Normalized PCE of the self-encapsulated *f*-PSCs measured after 7000 bending cycles at different bending radii (R = 3, 2, and 1.5 mm).


**Figure S13.** Photographs of the ultra-flexible and self-encapsulated devices (with the structure of PET/EVA/PET-PH1000/$NiO_x$/Pervoskite/EVA/PCBM/PEI/PET-PH1000/ PET/EVA) before and after crumpling test.

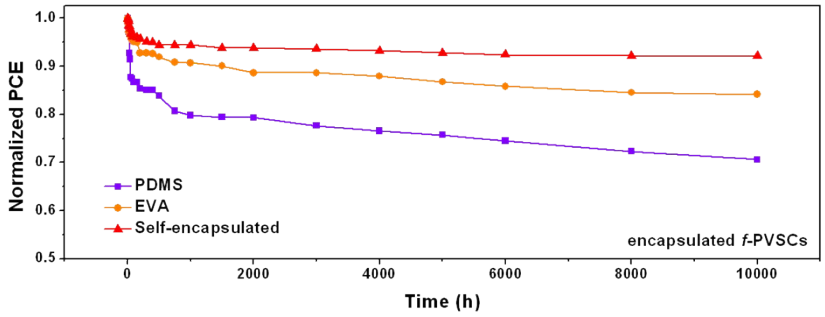


**Figure S14**. Long-term stability of the corresponding *f*-PSCs encapsulated by PDMS, EVA or self-encapsulation method upon storing in an enclosed conditions filled with water vapor (~ 80% humidity).

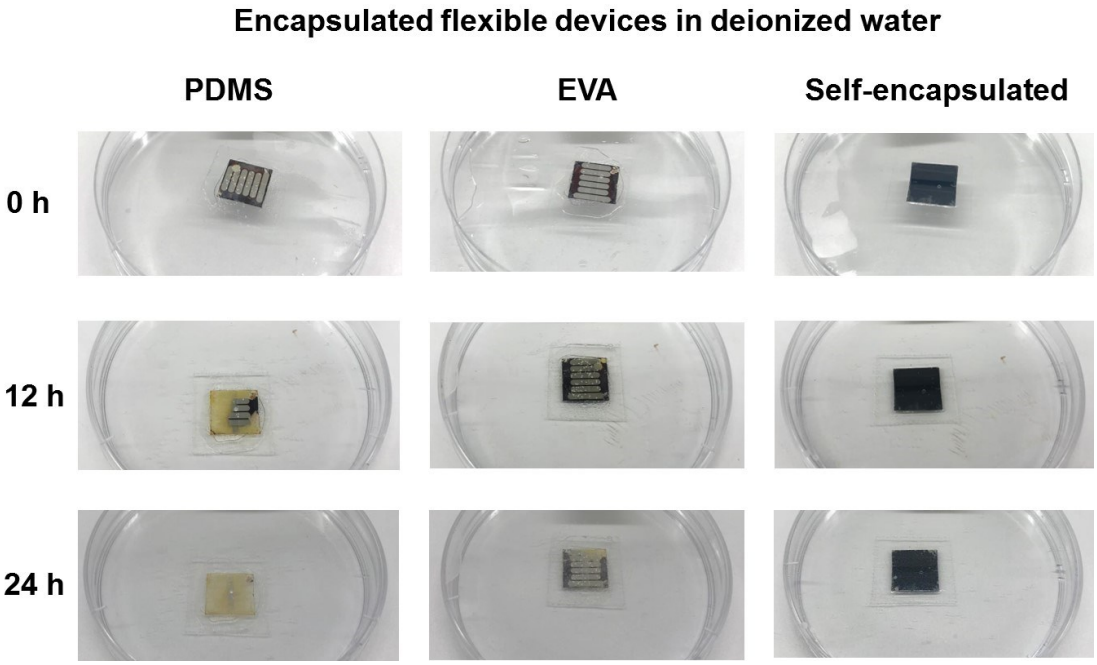


**Figure S15.** Water stability photographs of the flexible devices encapsulated by different methods.

**Table S1.** Several representative devices performance and structure of the laminated PSCs for comparision to this work.

| Device structure | Substrate | Electrode | PCE | Flexibility |
|---|---|---|---|---|
| FTO/$SnO_x$/laminated $MAPbI_3$ /$NiO_x$/FTO | Rigid | TCO | 10.6%[4] | - |
| ITO/PEDOT:PSS/$CH_3NH_3PbI_3$/ mp-$TiO_2$/c-$TiO_2$/FTO | Rigid | TCO | 6.9%[5] | - |
| FTO/c-$TiO_2$/mp-$TiO_2$/$CH_3NH_3PbI_3$/Sprio-OMeTAD/Au | Rigid | Au | 12.1%[6] (36.1$cm^2$) | - |
| FTO/ mp-$TiO_2$/$CH_3NH_3PbI_3$/ Sprio-OMeTAD/Au | Rigid | Au | 16.07%[7] | - |
| PEN foil/ITO/$SnO_x$/ $Cs_{0.1}(MA_{0.17}FA_{0.83})_{0.9}Pb(I_{0.83}Br_{0.17})_3$ /PTAA/$NiO_x$/Au/PEN foil | Flexible | Au | 11.3%[8] | - |
| **PET-EVA/PET-ITO/$NiO_x$/ $CH_3NH_3PbI_3$/EVA/PCBM/PEI/ PET-ITO/PET-EVA** | **Flexible** | **TCO** | **11.04%** | **Remain 95% of PCE for 1000 bending cycles at 0.5 mm radius, 81.2% for 100 crumpling cycles (this work)** |

**Table S2.** Summarized photovoltaic performance parameters of the self-encapsulated flexible PSCs.

| Device[a] | $J_{sc}$ (mA cm$^{-2}$) | $V_{oc}$ (V) | FF | PCE (%) |
|---|---|---|---|---|
| w/o EVA | 2.20±1.84 (4.04) | 0.87±0.05 (0.93) | 0.34±0.22 (0.58) | 1.15±1.05 (2.17) |
| with EVA | 11.47±1.55 (13.17) | 0.92±0.04 (0.96) | 0.30±0.19 (0.51) | 5.15±0.97 (6.42) |
| with EVA (PEI) | 18.94±0.98 (19.97) | 0.94±0.04 (0.96) | 0.40±0.17 (0.58) | 10.12±0.74 (11.04) |

a) The active area of the device is 0.19 cm$^2$. The average and standard deviation values are based on 24 cells.

**Table S3.** Young's modulus and thicknesses of the materials constituting the flexible perovskite solar cell.

| | PET/EVA | PET | PH1000 | $NiO_x$ | Perovskite | PCBM | PEI |
|---|---|---|---|---|---|---|---|
| Thickness (μm) | 2.6 | 2.5 | 0.12 | 0.02 | 0.4 | 0.06 | 0.01 |
| Young's modulus (Mpa) | 161 | 200 | 209 | 383 | 262 | 391 | 194 |

The neutral plane is defined by the equation below[9]:

$$b = \frac{\sum_{i=1}^{n} \overline{E}_i h_i \left[ \left( \sum_{j=1}^{i} h_j \right) - \frac{h_i}{2} \right]}{\sum_{i=1}^{n} \overline{E}_i h_i}$$

where $b$ is the distance from the top surface to neutral plane, $n$ is the total number of layers, $i$ is the index of each layer, $E_i$ and $h_i$ are the Young's modulus and the thickness of the $i^{th}$ layer, respectively.

For the conventional *f*-PSCs (n=6, PET/PH1000/$NiO_x$/Perovskite/PCBM/Ag: ~2.5μm/0.12μm/0.02μm/0.4μm/0.06μm/0.1μm), the neutral mechanical plane is 1.66 μm below the top surface (from the PET side), which is located at the PET substrate. For the self-encapsulated *f*-PSCs (n=10, PET/EVA/PET/PH1000/$NiO_x$/Perovskite/PCBM/PEI/PH1000/PET/EVA/PET: ~2.6μm/2.5μm/0.12μm/0.02μm/0.4μm/0.06μm/0.01μm/0.12μm/2.5μm/2.6μm), the neutral mechanical plane is 5.46 μm below the top surface, which is located at the perovskite layer.

**Table S4.** Several representative Pb leakage of PSCs for comparision to this work.

| Strategy | Pb concerntration | Reference |
|---|---|---|
| - | 2-2.7 mmol $L^{-1}$ under rainwater for 24 h | *Anal. Chem.* 2016, 88, 12316-12322 |
| Self-healing polymer-based encapsulation | 22 mg $m^{-2}$ under rainwater for 12 h; 130 mg $m^{-2}$ under rainwater for 72 h | *Nat. Energy* 2019, 4, 585-593 |
| Thiol-functionalized ZrL3 | 7.6 ppm in deionized water | *Nat. Nanotechnol.* 2020, 15, 934-940 |
| Lead-absorbing molecular coating on both sides of the deivces stack | 0.2 ppm in water | *Nature* 2020, 578, 555-558 |
| Cation-exchange resin | 14.3 ppb in water | *Nat. Energy* 2020, 5, 1003-1011. |
| **Flexible self-encapsulation** | **0.89 mg $L^{-1}$ in water for 24 h; 1.17 mg $L^{-1}$ for 200 cycles crumpling** | **This work** |

## Reference


1 F. Jiang, W. C. Choy, X. Li, D. Zhang, J. Cheng, *Adv. Mater.* 2015, **27**, 2930.

2 H. Zhang, J. Cheng, F. Lin, H. He, J. Mao, K. S. Wong, A. K.-Y. Jen, W. C. Choy, *ACS Nano* 2015, **10**, 1503.

3 Z. Huang, X. Hu, C. Liu, L. Tan, Y. Chen, *Adv. Funct. Mater.* 2017, **27**, 1703061.

4 S. P. Dunfield, D. T. Moore, T. R. Klein, D. M. Fabian, J. A. Christians, A. G. Dixon, B. Dou, S. Ardo, M. C. Beard, S. E. Shaheen, J. J. Berry, M. F. A. M. Van Hest, *ACS Energy Lett.* 2018, **3**, 1192.

5 L. Tan, C. Liu, Z. Huang, Y. Zhang, L. Chen, Y. Chen, *Org. Electron.* 2017, **48**, 308.

6 H. Chen, F. Ye, W. Tang, J. He, M. Yin, Y. Wang, F. Xie, E. Bi, X. Yang, M. Grätzel, L. Han, *Nature* 2017, **550**, 92.

7 J. Xiao, Y. Yang, X. Xu, J. Shi, L. Zhu, S. Lv, H. Wu, Y. Luo, D. Li, Q. Meng, *J. Mater. Chem. A* 2015, ***3***, 5289.

8 R. Schmager, J. Roger, J. A. Schwenzer, F. Schackmar, T. Abzieher, M. Malekshahi Byranvand, B. Abdollahi Nejand, M. Worgull, B. S. Richards, U. W. Paetzold, *Adv. Funct. Mater.* 2020, **30**, 1907481.

9 D.-H. Kim, J.-H. Ahn, W. M. Choi, H.-S. Kim, T.-H. Kim, J. Song, Y. Y. Huang, Z. Liu, C. Lu, J. A. Rogers, *Nature* 2008, **320**, 507-511.